Electronic Supplementary Information (ESI)†

for

Materials Design of High-capacity Li-rich Layered-Oxide Electrodes: Li_2MnO_3 and Beyond

Soo Kim,[a ||] Muratahan Aykol,[az ||] Vinay I. Hegde,[a ||] Zhi Lu,[a] Scott Kirklin,[a]

Jason R. Croy,[b] Michael M. Thackeray,[b] and Chris Wolverton*[a]

[a] *Department of Materials Science and Engineering, Northwestern University,*

2220 Campus Drive, Evanston, Illinois 60208, United States

[b] *Chemical Sciences and Engineering Division, Argonne National Laboratory,*

9700 South Cass Avenue, Argonne, Illinois 60439, United States

[z] *Current Address: Toyota Research Institute,*

4440 El Camino Real, Los Altos, California 94022, United States

*Correspondence: c-wolverton@northwestern.edu

[||] *These authors equally contributed to this work.*

Table S1. Thermodynamically stable and nearly-stable Li_2MO_3 compounds determined with a high-throughput density functional theory (HT-DFT) calculation within the OQMD framework.[33,34] The lowest DFT energy crystal structure, the formation energy, and the distance to the convex-hull are shown. A compound that is on the convex-hull of the Li-M-O system (*i.e.,* has a distance of ≤0 meV/atom from it) is considered stable. For all such stable compounds, the negative distances are given below, which measure the distance of the compound from the convex-hull excluding the compound itself, to merely provide an approximate measure of its stability. In addition, a distance on or within ~25 meV/atom of the convex-hull is to be considered as a nearly-stable compound.

Chemical compound	Lowest-energy crystal structure	Formation energy [eV/atom]	Distance to the convex-hull [meV/atom]	Stability
Li_2TiO_3	*C2/m*	-2.823	-77	Stable
Li_2VO_3	*C2/m*	-2.457	+23	Nearly-stable*
Li_2CrO_3	*C2/m*	-2.228	-15	Stable
Li_2MnO_3	*C2/c*†	-2.117	-115	Stable
Li_2FeO_3	*C2/m*	-1.855	-24	Stable
Li_2CoO_3	*C2/m*	-1.702	-60	Stable
Li_2NiO_3	*C2/m*	-1.519	-15	Stable
Li_2GeO_3	*Cmc21*	-2.186	+19	Nearly-stable**
Li_2ZrO_3	*Cc*	-2.879	+28	Nearly-stable**
Li_2MoO_3	*C2/m*	-2.203	+23	Nearly-stable*
Li_2RuO_3	*C2/c*†	-1.741	-67	Stable
Li_2RhO_3	*C2/m*	-1.644	-92	Stable
Li_2PdO_3	*C2/m*	-1.512	-100	Stable
Li_2SnO_3	*C2/m*	-2.130	-107	Stable
Li_2HfO_3	*C2/m*	-3.028	-119	Stable
Li_2OsO_3	*C2/m*	-1.708	-24	Stable
Li_2IrO_3	*C2/m*	-1.611	-45	Stable
Li_2PtO_3	*C2/m*	-1.564	-91	Stable
Li_2PbO_3	*C2/c*†	-1.674	-29	Stable

† The *C2/c* structure is very similar to the *C2/m* structure: both are monoclinic, with six-fold and three-fold axes of symmetry respectively. Therefore, for the purposes of this study, we do not distinguish between these two structures.

* According to our DFT calculations, we find that both Li_2MoO_3 and Li_2VO_3 decompose to other stable phase (or phase mixtures). We find this to be consistent with *Ref.* 21, where Li_2MoO_3 decomposes to amorphous Li_2MoO_4 and MoO_3 when exposed to air. In *Ref.* 47, Li_2VO_3 was synthesized by a high-energy-ball-milling technique to yield a disordered cubic $Fm\bar{3}m$ structure.

** There are other polymorphs that we find them to be more stable in our OQMD database[33,34] for Li_2GeO_3 (*Cmc21*)[48] and Li_2ZrO_3 (*Cc*)[25]. Since the formation energies between these crystal structures and *C2/m* Li_2MO_3 are very close (within ~25 meV/atom), we believe that Li_2GeO_3 and Li_2ZrO_3 in *C2/m* structures can be synthesized when the experiments are designed carefully in order to find suitable synthesis conditions.

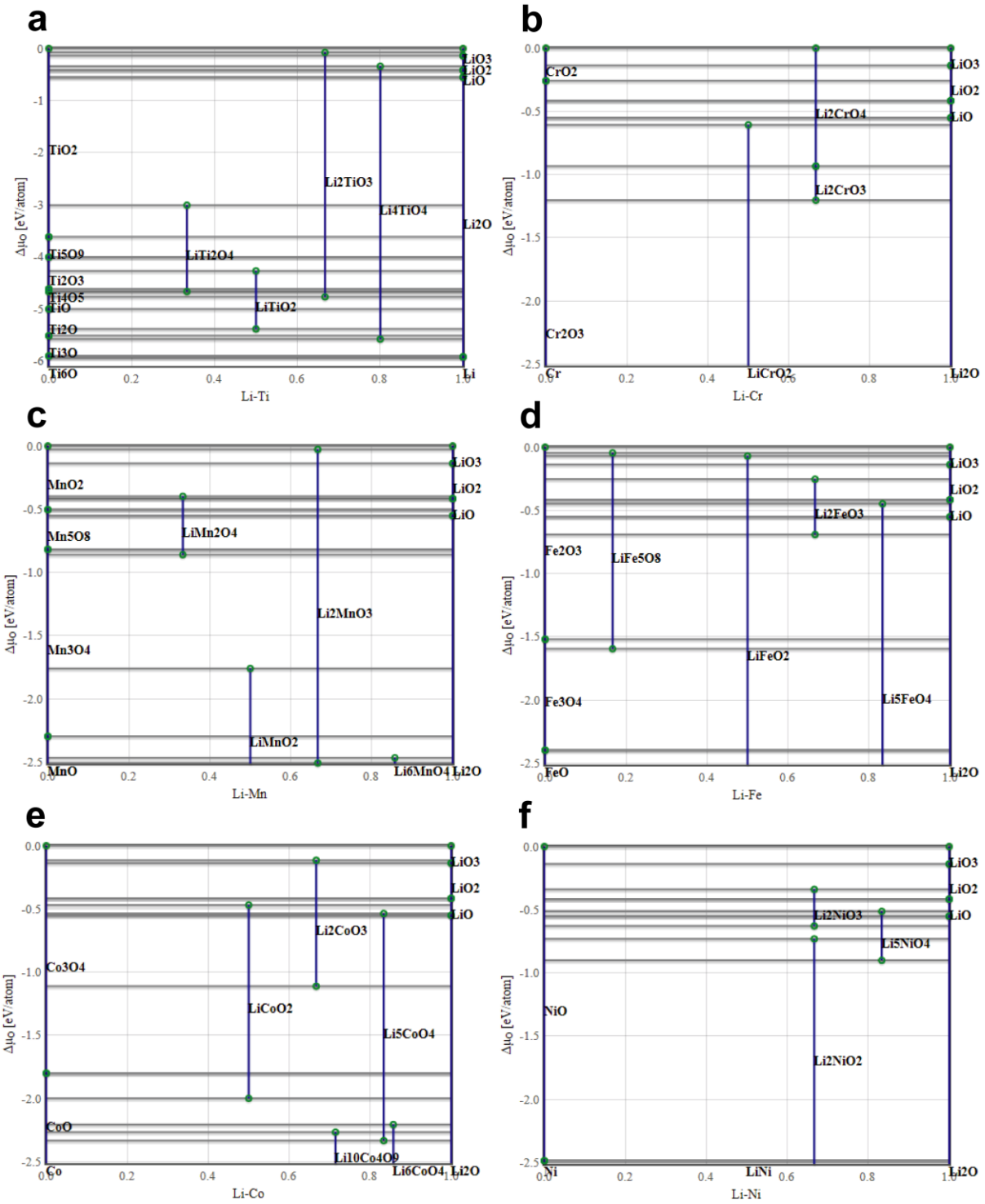

Figure S1. Critical oxygen chemical potential plots of Li_2MO_3 compounds: The stabilities of the Li_2MO_3 species with varying oxygen chemical potentials are shown. Each compound has the lower and upper limits of the oxygen chemical potentials, where it can decompose to other stable phase mixtures outside of this window. Critical oxygen chemical potential plots of: a) Li_2TiO_3, b) Li_2CrO_3, c) Li_2MnO_3, d) Li_2FeO_3, e) Li_2CoO_3, f) Li_2NiO_3.

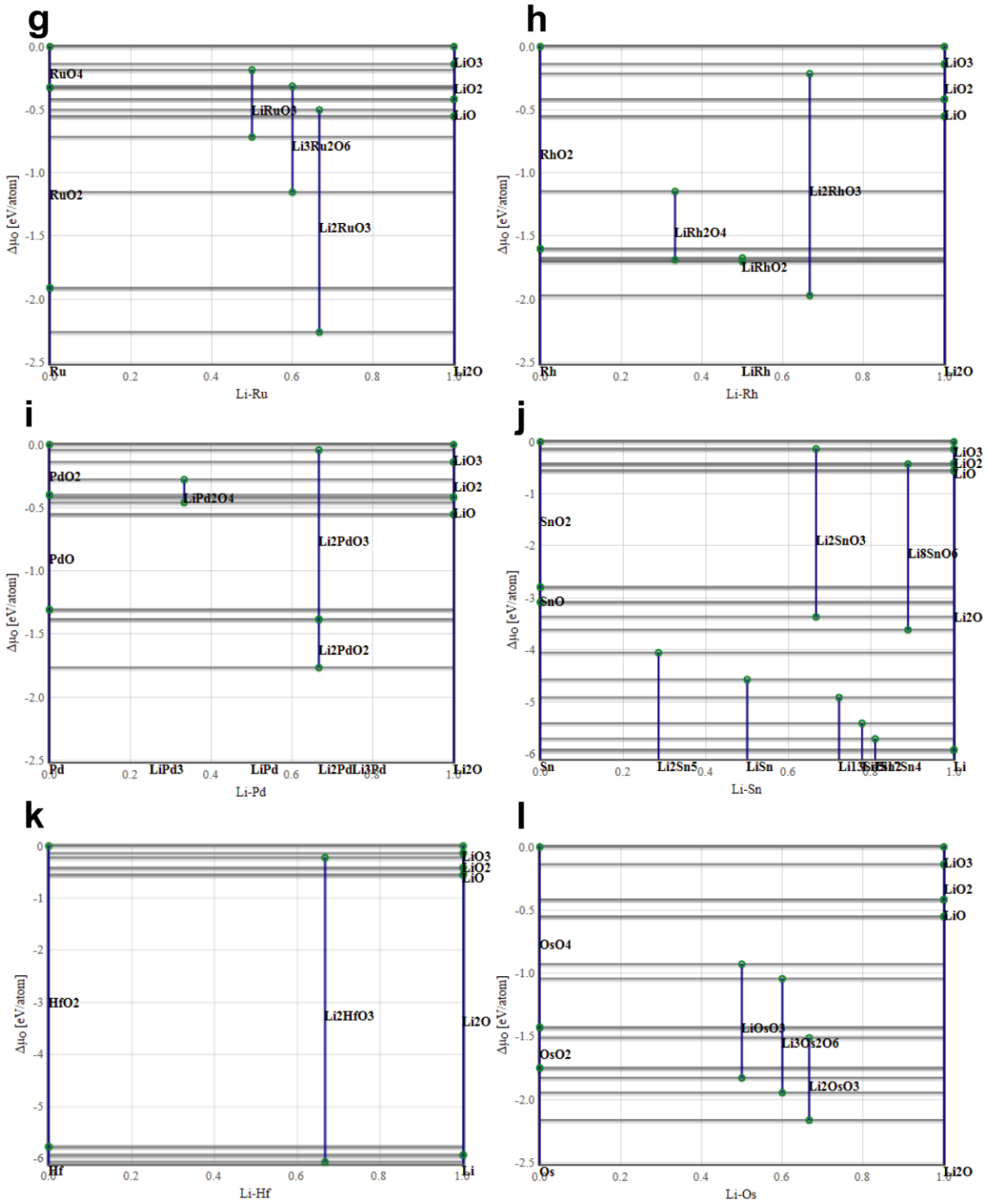

Figure S1. (*cont.*) g) Li_2RuO_3, h) Li_2RhO_3, i) Li_2PdO_3, j) Li_2SnO_3, k) Li_2HfO_3, l) Li_2OsO_3.

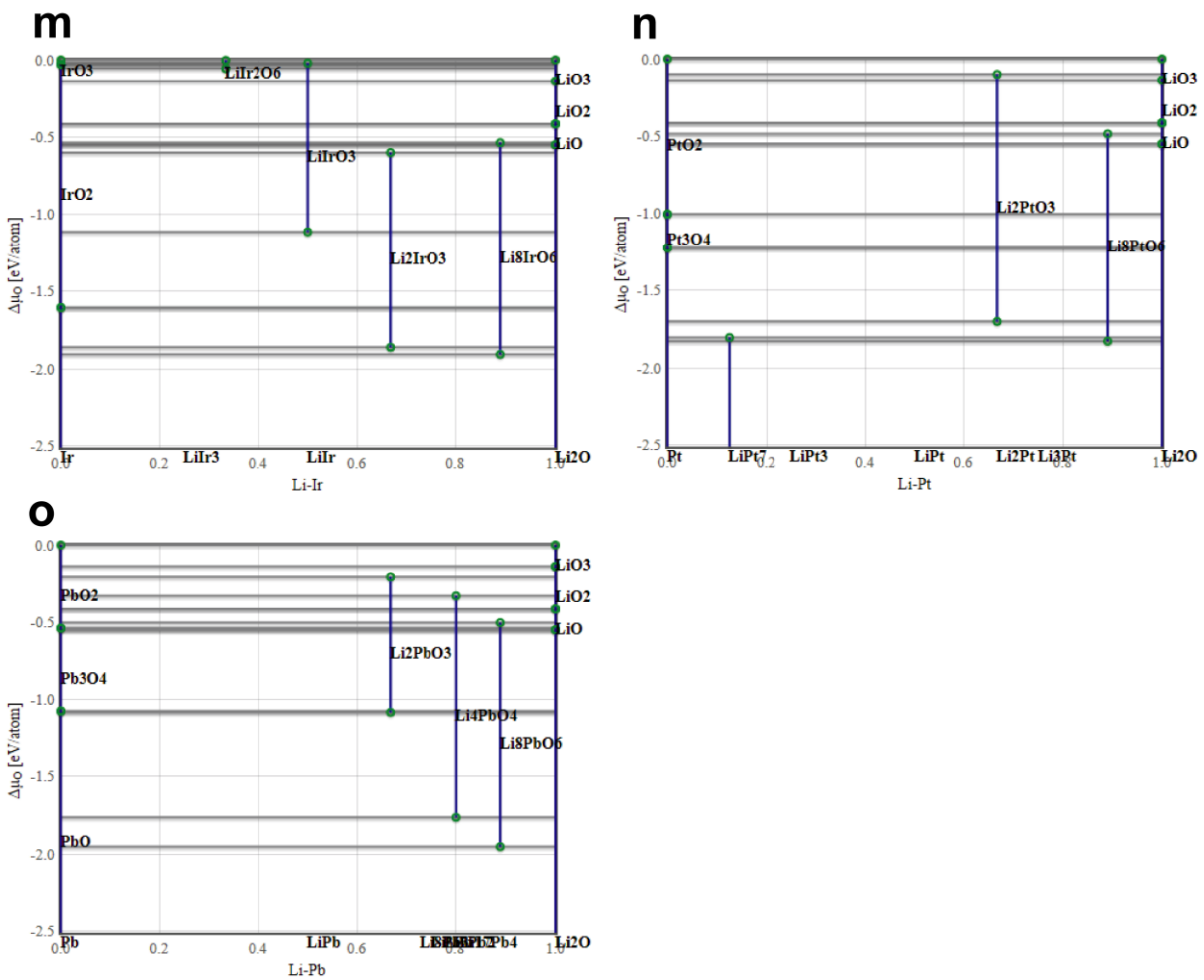

Figure S1. (*cont.*) m) Li_2IrO_3, n) Li_2PtO_3, and o) Li_2PbIrO_3. We observe relatively narrow oxygen chemical potential windows for Li_2CrO_3, Li_2FeO_3, Li_2NiO_3, and Li_2OsO_3 in panels b), d), f), and l), respectively. These compounds may be more difficult to be synthesized. For example, we predict that Li_2CrO_3 may contain impurities such as $LiCrO_2$ in the oxygen-deficient condition and Li_2CrO_4 in the oxygen-rich condition, as shown in panel b). Similarly, Li_2FeO_3 may contain impurities such as Li_5FeO_4 and $LiFeO_2$, as shown in panel d); and, Li_2NiO_3 and Li_2OsO_3 may contain impurities such as Li_2NiO_2 and $Li_3Os_2O_6$ during the synthesis [see panels f) and l), respectively].

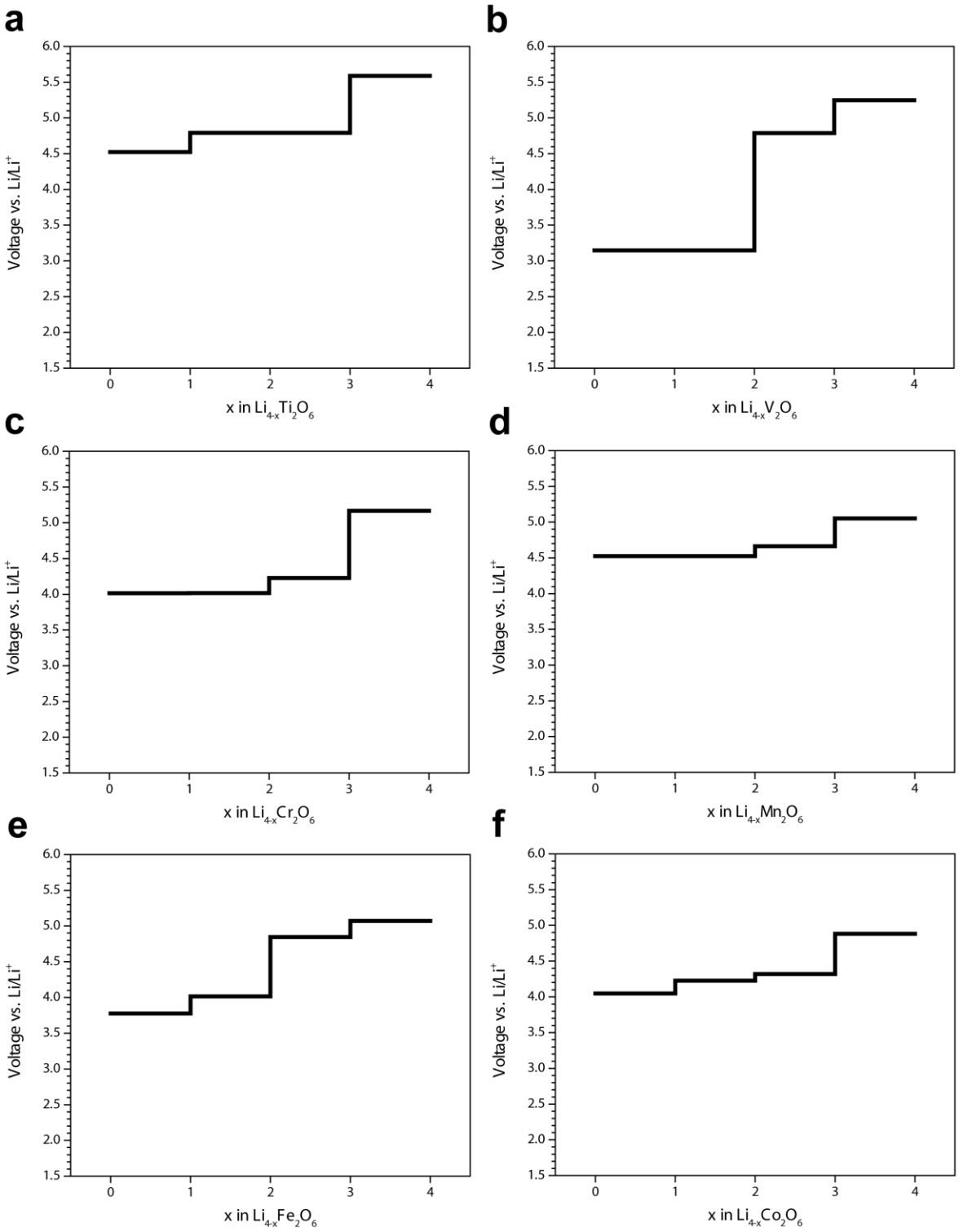

Figure S2. Calculated voltage steps of Li_2MO_3: We have considered the following delithiation steps: $Li_4M_2O_6 \rightarrow Li_3M_2O_6 \rightarrow Li_2M_2O_6 \rightarrow M_2O_6$ and report the reactions with the stable intermediate species with respect to the Li_2MO_3-MO_3 convex-hull. Calculated voltage steps of: a) Li_2TiO_3, b) Li_2VO_3, c) Li_2CrO_3, d) Li_2MnO_3, e) Li_2FeO_3, f) Li_2CoO_3.

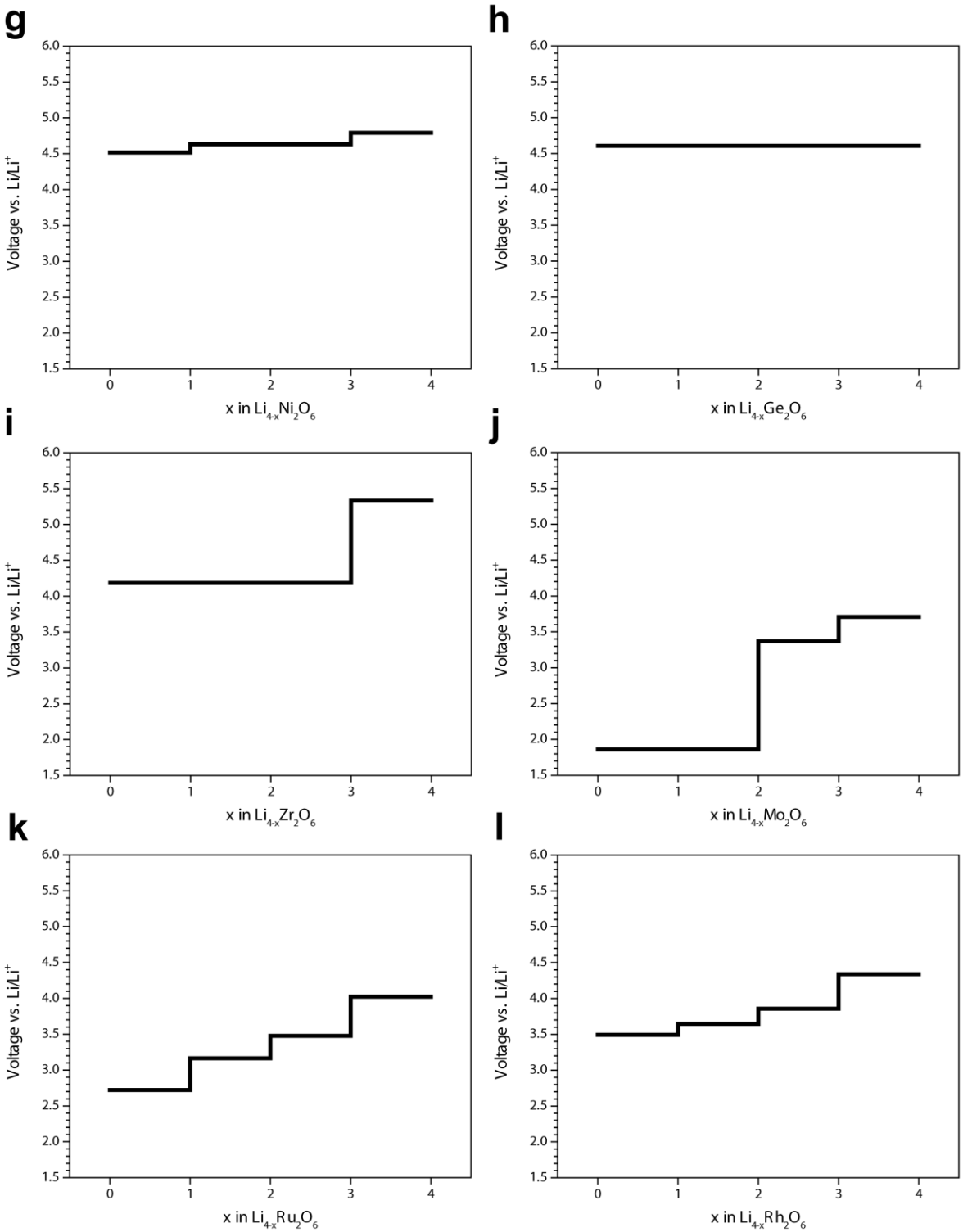

Figure S2. (*cont.*) g) Li_2NiO_3, h) Li_2GeO_3, i) Li_2ZrO_3, j) Li_2MoO_3, k) Li_2RuO_3, l) Li_2RhO_3.

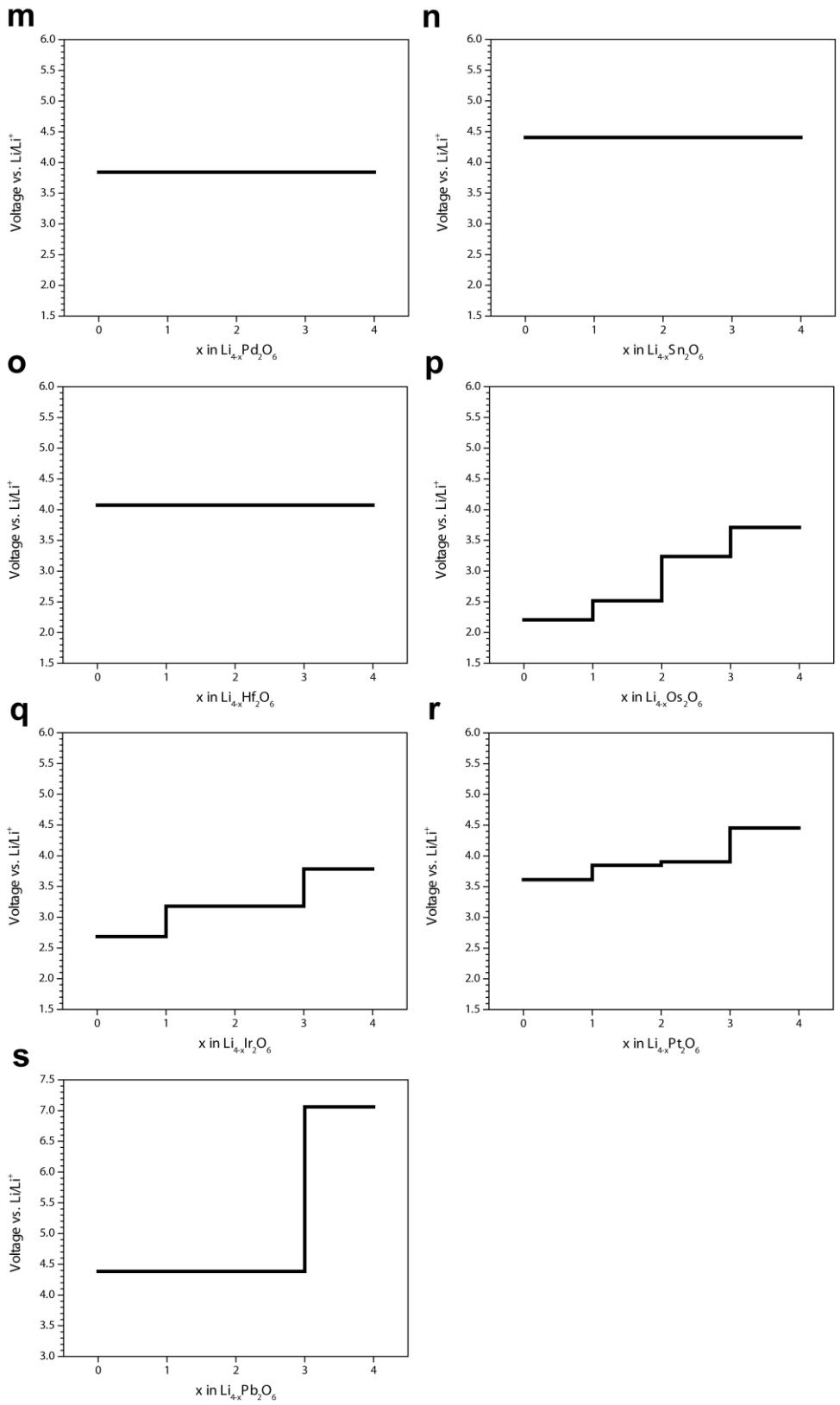

Figure S2. (*cont.*) m) Li_2PdO_3, n) Li_2SnO_3, o) Li_2HfO_3, p) Li_2OsO_3, q) Li_2IrO_3, r) Li_2PtO_3, and s) Li_2PbO_3 (please note a different y-axis scaling for panel s).

Table S2. Stable and nearly-stable delithiated cathode structures: These cathode structures will be more stable against decomposition into other phases during charging process.

Stable $Li_{2-x}MO_3$ cathodes	**Nearly-stable $Li_{2-x}MO_3$ cathodes**
$Li_{1.5}RuO_3$	$LiRuO_3$
$Li_{1.5}OsO_3$	$Li_{0.5}RuO_3$
$Li_{0.5}IrO_3$	RuO_3
IrO_3	$Li_{1.5}RhO_3$
	$LiRhO_3$
	$LiOsO_3$
	$Li_{0.5}OsO_3$
	OsO_3
	$Li_{1.5}IrO_3$
	$Li_{1.5}PtO_3$
	$LiPtO_3$

Table S3. Oxygen vacancy formation energy: We have removed the lowest energy oxygen atom in the DFT supercell in order to calculate the oxygen vacancy formation energy for Li_2MO_3, $Li_{1.5}MO_3$ and MO_3 cathode compounds.

Chemical compound	**$Li_8M_4O_{12}$ to $Li_8M_4O_{11}$ [eV/vacancy]**	**$Li_6M_4O_{12}$ to $Li_6M_4O_{11}$ [eV/vacancy]**	**M_4O_{12} to M_4O_{11} [eV/vacancy]**
Li_2TiO_3	5.772	-1.362	-8.927
Li_2VO_3	4.337	0.830	-2.502
Li_2CrO_3	2.490	1.028	-3.742
Li_2MnO_3	2.548	0.481	-1.620
Li_2FeO_3	0.726	0.228	-2.036
Li_2CoO_3	2.347	0.996	-0.023
Li_2NiO_3	0.900	0.044	-0.325
Li_2GeO_3	4.902	-1.054	-3.768
Li_2ZrO_3	6.569	-1.176	-7.238
Li_2MoO_3	4.631	4.377	0.711
Li_2RuO_3	2.934	3.033	0.287
Li_2RhO_3	2.522	2.061	-0.071
Li_2PdO_3	1.992	1.092	0.170
Li_2SnO_3	4.120	-1.546	-3.251
Li_2HfO_3	6.882	-0.977	-1.457
Li_2OsO_3	3.278	3.276	1.341
Li_2IrO_3	2.592	2.714	2.046
Li_2PtO_3	2.225	1.925	0.851
Li_2PbO_3	1.997	-1.624	-10.481

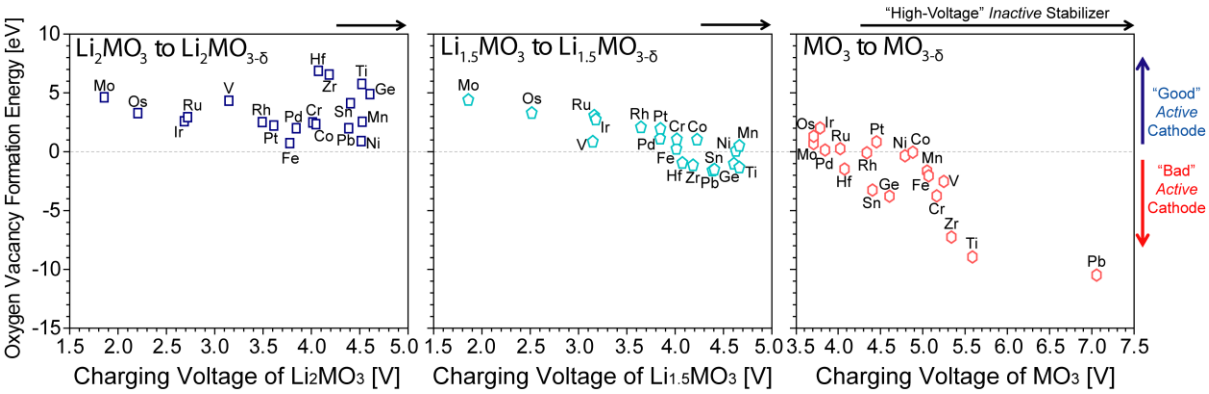

Figure S3. Oxygen vacancy formation energies (per vacancy) *vs.* delithiation voltages of Li_2MO_3 ($Li_8M_4O_{12}$), $Li_{2-\delta}MO_3$ ($Li_6M_4O_{12}$), and MO_3 (M_4O_{12}) cathode materials: Every possible oxygen sites in the DFT cells are evaluated to remove the lowest energy oxygen atom for each composition. The *x*-axis indicates the delithiation voltage at each composition of cathode compounds adapted from Fig. 2. Here, it is possible to determine at which voltage the oxygen loss occurs for each $Li_{2-x}MO_3$ system (*i.e.*, when $\Delta E_{vac,O}$ becomes negative). The oxygen vacancy formation energies are subtracted by the oxygen chemical potential corresponding to 300 K.

Table S4. Metal-migration tendency in $Li_{1.5}MO_3$, $Li_{1.5}MO_{3-\delta}$, MO_3, and $MO_{3-\delta}$: The DFT formation energy (ΔH_f) was calculated for both the pristine-structure (PS) and the metal-migrated-structure (MMS). For MMS, the metal was placed to the energetically most favorable empty Li-site. The positive energy difference indicates the MMS is thermodynamically preferred, while the negative energy difference shows that the PS is the stable configuration.

$Li_{1.5}MO_3$	ΔH_f, PS-$Li_6M_4O_{12}$ [eV/atom]	ΔH_f, MMS-$Li_6M_4O_{12}$ [eV/atom]	$(\Delta H_{f,MMS} - \Delta H_{f,PS}) \times \frac{22}{4}$ [eV/metal]
Ti	-2.668	-2.649	0.105
V	-2.378	-2.362	0.088
Cr	-2.065	-2.057	0.044
Mn	-1.893	-1.824	0.380
Fe	-1.680	-1.597	0.457
Co	-1.489	-1.401	0.484
Ni	-1.244	-1.153	0.501
Ge	-1.941	-1.857	0.462
Zr	-2.740	-2.741	-0.005
Mo	-2.226	-2.189	0.204
Ru	-1.650	-1.532	0.649
Rh	-1.473	-1.453	0.110
Pd	-1.266	-1.140	0.693
Sn	-1.893	-1.869	0.132
Hf	-2.897	-2.877	0.110
Os	-1.663	-1.541	0.671
Ir	-1.510	-1.374	0.748
Pt	-1.370	-1.240	0.715
Pb	-1.415	-1.391	0.132

Table S4. (*cont.*) Metal-migration tendency in $Li_{1.5}MO_{3-\delta}$.

$Li_{1.5}MO_{3-\delta}$	ΔH_f, PS-$Li_6M_4O_{11}$ [eV/atom]	ΔH_f, MMS-$Li_6M_4O_{11}$ [eV/atom]	$(\Delta H_{f,MMS} - \Delta H_{f,PS}) \times \frac{21}{4}$ [eV/metal]
Ti	-2.828	-2.815	0.068
V	-2.429	-2.416	0.068
Cr	-2.095	-2.154	-0.310
Mn	-1.939	-1.887	0.273
Fe	-1.725	-1.660	0.341
Co	-1.497	-1.395	0.535
Ni	-1.278	-1.194	0.441
Ge	-2.049	-1.991	0.304
Zr	-2.913	-2.829	0.441
Mo	-2.089	-1.810	1.465
Ru	-1.556	-1.485	0.373
Rh	-1.411	-1.356	0.289
Pd	-1.240	-1.164	0.399
Sn	-2.019	-1.930	0.467
Hf	-3.047	-2.954	0.488
Os	-1.551	-1.500	0.268
Ir	-1.418	-1.347	0.373
Pt	-1.309	-1.234	0.394
Pb	-1.525	-1.467	0.304

Table S4. (*cont.*) Metal-migration tendency in MO_3.

MO_3	ΔH_f, PS-M_4O_{12} [eV/atom]	ΔH_f, MMS-M_4O_{12} [eV/atom]	$(\Delta H_{f,MMS} - \Delta H_{f,PS}) \times \frac{16}{4}$ [eV/metal]
Ti	-1.772	-2.113	-1.364
V	-1.644	-1.656	-0.048
Cr	-1.163	-1.246	-0.332
Mn	-0.828	-0.817	0.044
Fe	-0.569	-0.830	-1.044
Co	-0.368	-0.417	-0.196
Ni	0.040	-0.016	-0.224
Ge	-0.976	-1.097	-0.484
Zr	-2.086	-2.492	-1.624
Mo	-1.955	-2.076	-0.484
Ru	-0.936	-0.909	0.108
Rh	-0.545	-0.516	0.116
Pd	-0.345	-0.328	0.068
Sn	-0.992	-1.067	-0.300
Hf	-2.505	-2.695	-0.760
Os	-1.103	-1.077	0.104
Ir	-0.809	-0.782	0.108
Pt	-0.357	-0.347	0.040
Pb	-0.595	-0.714	-0.476

Table S4. (*cont.*) Metal-migration tendency in $MO_{3-\delta}$.

$MO_{3-\delta}$	ΔH_f, PS-M_4O_{11} [eV/atom]	ΔH_f, MMS-M_4O_{11} [eV/atom]	$(\Delta H_{f,MMS} - \Delta H_{f,PS}) \times \frac{15}{4}$ [meV/metal]
Ti	-2.445	-2.418	0.101
V	-1.893	-1.889	0.015
Cr	-1.472	-1.436	0.135
Mn	-0.965	-0.992	-0.101
Fe	-0.713	-0.907	-0.728
Co	-0.366	-0.373	-0.026
Ni	0.045	-0.510	-2.081
Ge	-1.249	-1.244	0.019
Zr	-2.690	-2.685	0.019
Mo	-2.019	-2.030	-0.041
Ru	-0.935	-0.958	-0.086
Rh	-0.543	-0.574	-0.116
Pd	-0.313	-0.326	-0.049
Sn	-1.226	-1.235	-0.034
Hf	-2.725	-2.822	-0.364
Os	-1.043	-1.064	-0.079
Ir	-0.682	-0.774	-0.345
Pt	-0.281	-0.297	-0.060
Pb	-0.634	-0.765	-0.491

Table S5. Properties of Li_2MO_3 predicted from HT-DFT calculations.

Li_2MO_3	Pros.	Cons.	Classification
Ti	ⓢⓥⓜ	ⓓⓞ	stabilizer
V	ⓞⓜ	ⓢⓓ	active cathode
Cr	ⓞⓜ	ⓢⓓ	stabilizer/active cathode
Mn	ⓢⓥ	ⓓⓜ	stabilizer
Fe	$	ⓢⓓⓞⓜ	stabilizer
Co	ⓞ	ⓓⓜ	stabilizer/active cathode
Ni	ⓥ$	ⓓⓢⓞⓜ	stabilizer
Ge	ⓥⓜ	ⓢ	stabilizer
Zr	ⓥ	ⓓⓢ	stabilizer
Mo	ⓞ	ⓢⓓⓜ	active cathode
Ru	ⓓⓞⓜ	$	active cathode
Rh	ⓢⓓⓞⓜ	$	stabilizer/active cathode
Pd	ⓢⓞⓜ	$	stabilizer/active cathode
Sn	ⓢⓥ	ⓞⓜ	stabilizer
Hf	ⓢ	ⓞⓜ	stabilizer
Os	ⓓⓞⓜ	ⓢ$	active cathode
Ir	ⓓⓞⓜ	$	active cathode
Pt	ⓢⓓⓞⓜ	$	stabilizer/active cathode
Pb	ⓥ	ⓓⓞⓜ	stabilizer

ⓢsynthesizability↑ ⓥhigh-voltage stabilizer ⓓstable delithiation product ⓞoxygen stability↑ ⓜmigration↓ $abundant
ⓢsynthesizability↓ ⓥlow-voltage stabilizer ⓓmetastable delithiation product ⓞoxygen stability↓ ⓜmigration↑ $cost↑

Table S6. Mixing energies in $Li_4M_IM_{II}O_6$ compounds [meV/site]†.

	Ti	V	Cr	Mn	Fe	Co	Ni	Ge	Zr	Mo	Ru	Rh	Pd	Sn	Hf	Os	Ir	Pt	Pb
Ti	n/a	-4.6	0.9	-2.7	11	13	5	14	-14	41	5.0	9.7	3.4	22	-5.8	13	10	2.8	36
V	-4.6	n/a	-44	5.5	-58	-45	-57	14	1.9	2.2	20	-5	15	27	9.4	18	25	13	35
Cr	0.9	-44	n/a	2.5	2.4	-0.6	2.7	5.5	7.4	-74	-47	3.2	12	20	14	-75	-32	5.7	32
Mn	-2.7	5.5	2.5	n/a	5.2	11	0.5	-0.5	6.9	-69	17	14	4.5	14	12	-8.3	11	-0.1	22
Fe	11	-58	2.4	5.2	n/a	4.5	-3.2	2.4	5.1	-134	-62	-20	21	14	12	-89	-52	-16	22
Co	13	-45	-0.6	11	4.5	n/a	-5.9	2.2	25	-154	-52	6.2	12	94	30	-80	-26	5.5	36
Ni	5	-57	2.7	0.5	-3.2	-5.9	n/a	-7.3	21	-254	-89	-24	2.9	14	25	-175	-117	-23	22
Ge	14	14	5.5	-0.5	2.4	2.2	-7.3	n/a	23	76	8.2	1.7	-12	7.7	29	31	0.9	-17	16
Zr	-14	1.9	7.4	6.9	5.1	25	21	23	n/a	48	5.3	6.5	-1.2	15	-9.4	20	3.8	-6.6	19
Mo	41	2.2	-74	-69	-134	-154	-254	76	48	n/a	-59	-49	-8.4	74	61	-24	-25	61	-72
Ru	5.0	20	-47	17	-62	-52	-89	8.2	5.3	-59	n/a	-25	13	17	18	3.2	-3.4	22	-10
Rh	9.7	-5	3.2	14	-20	6.2	-24	1.7	6.5	-49	-25	n/a	12	11	14	-40	-13	9.3	0.5
Pd	3.4	15	12	4.5	21	12	2.9	-12	-1.2	-8.4	13	12	n/a	-5.3	6.2	6.0	5.1	-5.2	-10
Sn	22	27	20	14	14	94	14	7.7	15	74	17	11	-5.3	n/a	23	40	9.4	-13	0.4
Hf	-5.8	9.4	14	12	12	30	25	29	-9.4	61	18	14	6.2	23	n/a	38	16	2.1	29
Os	13	18	-75	-8.3	-89	-80	-175	31	20	-24	3.2	-40	6.0	40	38	n/a	1	51	-33
Ir	10	25	-32	11	-52	-26	-117	0.9	3.8	-25	-3.4	-13	5.1	9.4	16	1	n/a	17	-19
Pt	2.8	13	5.7	-0.1	-16	5.5	-23	-17	-6.6	61	22	9.3	-5.2	-13	2.1	51	17	n/a	-25
Pb	36	35	32	22	22	36	22	16	19	-72	-10	0.5	-10	0.4	29	-33	-19	-25	n/a

† An ordered $Li_4M_IM_{II}O_6$ compound can be formed when the calculated DFT mixing energy is found to be very negative. There is a previous study that high capacity can be achieved in disordered structure.[19] However, there have not been sufficient studies at the present time to exclude all ordered compounds to be used in LIB applications. Predicting the electrochemical performance for all of the compounds listed in Table S6 is beyond the scope of current study.

Table S7. Stable II-VI and III-V $Li_4M_IM_{II}O_6$ compounds (and possible oxidation states)

II-VI compounds
Li_4CoTeO_6 (2-6, 4-4)
Li_4MnTeO_6 (2-6, 4-4)
Li_4NiTeO_6 (2-6, 4-4)
Li_4ZnTeO_6 (2-6)

III-V compounds
Li_4AlIrO_6 (3-5)
Li_4AlOsO_6 (3-5)
Li_4AlPtO_6 (3-5)
Li_4AlRhO_6 (3-5)
Li_4AlRuO_6 (3-5)
Li_4AlSbO_6 (3-5)
Li_4CoBiO_6 (3-5)
Li_4CoSbO_6 (3-5)
Li_4CrBiO_6 (3-5)
Li_4CrSbO_6 (3-5)
Li_4CuOsO_6 (3-5)
Li_4DyOsO_6 (3-5)
Li_4ErOsO_6 (3-5)
Li_4FeSbO_6 (3-5)
Li_4GaOsO_6 (3-5)
Li_4GaRuO_6 (3-5)
Li_4GaIrO_6 (3-5)
Li_4GdOsO_6 (3-5)
Li_4HoOsO_6 (3-5)
Li_4InBiO_6 (3-5)
Li_4InOsO_6 (3-5)
Li_4InSbO_6 (3-5)
Li_4MnSbO_6 (3-5)
Li_4NiSbO_6 (3-5)
Li_4SbRhO_6 (3-5)
Li_4ScOsO_6 (3-5)
Li_4TbOsO_6 (3-5)
Li_4TlOsO_6 (3-5)
Li_4YOsO_6 (3-5)

Table S8. Nearly Stable II-VI and III-V $Li_4M_IM_{II}O_6$ compounds (oxidation states)

II-VI compounds
Li_4FeTeO_6 (2-6, 4-4)
Li_4NiWO_6 (2-6)

III-V compounds
Li_4AlBiO_6 (3-5)
Li_4BiOsO_6 (3-5)
Li_4CeOsO_6 (3-5)
Li_4CoNbO_6 (3-5)
Li_4CoTaO_6 (3-5)
Li_4CrNbO_6 (3-5)
Li_4CrTaO_6 (3-5)
Li_4FeNbO_6 (3-5)
Li_4FeTaO_6 (3-5)
Li_4GaBiO_6 (3-5)
Li_4GaPtO_6 (3-5)
Li_4GaRhO_6 (3-5)
Li_4GaSbO_6 (3-5)
Li_4MnTaO_6 (3-5)
Li_4NiBiO_6 (3-5)
Li_4NiTaO_6 (3-5)
Li_4ScBiO_6 (3-5)
Li_4ScNbO_6 (3-5)
Li_4ScSbO_6 (3-5)
Li_4ScTaO_6 (3-5)
Li_4SmOsO_6 (3-5)
Li_4TaRhO_6 (3-5)
Li_4TlBiO_6 (3-5)
Li_4TlSbO_6 (3-5)
Li_4VNbO_6 (3-5)
Li_4VSbO_6 (3-5)
Li_4VTaO_6 (3-5)

Table S9. Calculated lattice parameters for Li_2MO_3 compounds using HT-DFT: We used $Li_4M_2O_6$ primitive cells to calculate the lattice parameters in *C2/m* monoclinic crystal structures. Then, we converted these values to the hexagonal $R\bar{3}m$ structure, where the lattice parameter *a* indicates the distance between two adjacent lithium atom and the lattice parameter *c* is the interlayer spacing in the *z*-direction (see the schematic below Table S9). We have provided $R\bar{3}m$ *c*/*a* ratio in Table S9, which is a direct measure of layered characteristic for the cathode materials (also, see Fig. S4).

Chemical compound	***C2/m* crystal structure**						**Refined to $R\bar{3}m$**		
	***a* [Å]**	***b* [Å]**	***c* [Å]**	***α* [°]**	***β* [°]**	***γ* [°]**	***a* [Å]**	***c* [Å]**	***c/a***
Li_2TiO_3	5.064	8.748	5.074	90.0	109.7	90.0	2.916	14.327	4.913
Li_2VO_3	4.952	8.772	4.997	90.0	108.4	90.0	2.924	14.222	4.864
Li_2CrO_3	5.007	8.524	5.019	90.0	110.2	90.0	2.841	14.134	4.975
Li_2MnO_3	4.933	8.532	4.994	90.0	109.5	90.0	2.844	14.120	4.965
Li_2FeO_3	4.917	8.689	4.981	90.0	108.5	90.0	2.896	14.173	4.894
Li_2CoO_3	4.906	8.616	4.954	90.0	108.7	90.0	2.872	14.077	4.901
Li_2NiO_3	4.825	8.350	4.919	90.0	109.1	90.0	2.783	13.943	5.010
Li_2GeO_3	4.969	8.597	5.054	90.0	109.4	90.0	2.866	14.298	4.989
Li_2ZrO_3	5.392	9.293	5.226	90.0	110.3	90.0	3.098	14.704	4.747
Li_2MoO_3	5.132	8.511	5.199	90.0	108.5	90.0	2.837	14.789	5.213
Li_2RuO_3	5.035	8.702	5.116	90.0	109.2	90.0	2.901	14.494	4.997
Li_2RhO_3	5.075	8.766	5.079	90.0	109.7	90.0	2.922	14.349	4.911
Li_2PdO_3	5.118	8.841	5.080	90.0	109.8	90.0	2.947	14.338	4.865
Li_2SnO_3	5.319	9.184	5.229	90.0	110.1	90.0	3.061	14.733	4.813
Li_2HfO_3	5.337	9.200	5.203	90.0	110.3	90.0	3.067	14.644	4.775
Li_2OsO_3	5.177	8.436	5.159	90.0	109.4	90.0	2.812	14.600	5.192
Li_2IrO_3	5.100	8.795	5.104	90.0	109.7	90.0	2.932	14.420	4.919
Li_2PtO_3	5.178	8.934	5.046	90.0	110.2	90.0	2.978	14.204	4.770
Li_2PbO_3	5.474	9.473	5.302	90.0	110.1	90.0	3.158	14.937	4.730

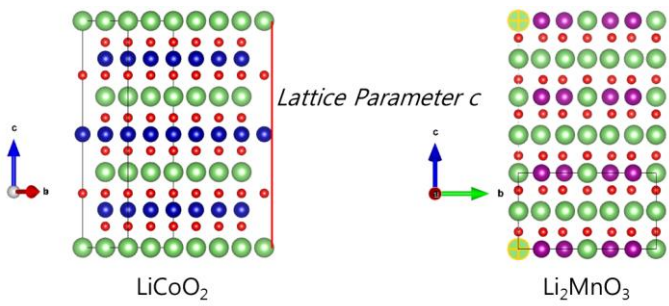

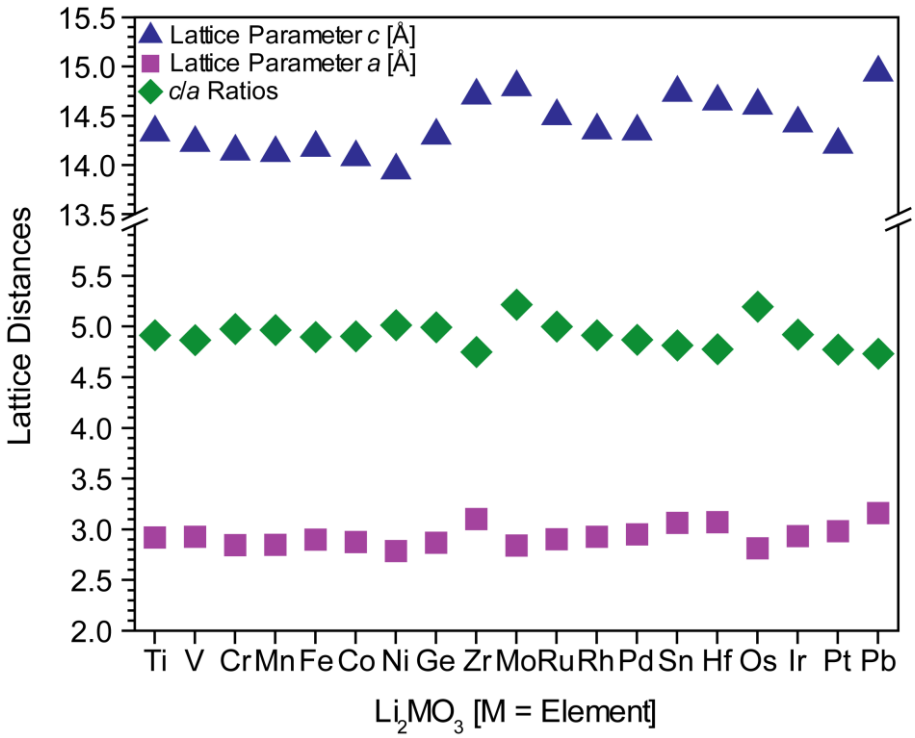

Figure S4. Lattice parameters of Li_2MO_3 compounds: The *C2/m* monoclinic Li_2MO_3 lattice parameters have been converted to the hexagonal $R\bar{3}m$ structure, and the lattice parameters *a* and *c* are provided. The *c*/*a* ratios are also provided. Comparing the $R\bar{3}m$ $LiNi_{0.5}Co_{0.2}Mn_{0.3}O_2$ and $LiCoO_2$ cathode materials with Li_2MnO_3, there are ~1% differences in the lattice parameters.[75,76] Between the Li_2RuO_3 and Li_2SnO_3 compounds in Fig. S4, there is 0.161 Å difference in the lattice parameter *a* and 0.239 Å difference in the lattice parameter *c*. Overall, we find that the lattice mismatch in the lattice parameters *a* is quite small (< 0.4 Å), while the differences of the lattice parameters *c* can be up to ~1 Å. We believe that it would not be beneficial not to have a large mismatch in *z*-direction. For instance, we do not recommend incorporating Li_2NiO_3 with Li_2MoO_3, Li_2SnO_3, or Li_2PbO_3. In addition, the most of the Li_2MO_3 compounds shown in Fig. S4 have the lattice parameter *c* less than 14.6 Å, which could be experimentally tested with the common $R\bar{3}m$ cathode compounds that the typical lattice distance in z-direction varies between 14.0 to 14.3 Å.[75,76] Lastly, the *c*/*a* ratio for typical $R\bar{3}m$ layered compounds is approximately ~5,[75,76] which the most of new Li_2MO_3 may match this criteria.

Table S10. Suggested active/active cathode pairs†.

M in Li_2MO_3	active/active Li_2MO_3 cathode pairs
Cr	Co, Ru, Rh, Pt
Co	Cr, Rh
Ru	Cr, Rh, Pd, Os, Ir, Pt
Rh	Cr, Co, Ru, Pd, Os, Ir, Pt
Pd	Ru, Rh, Pt
Os	Ru, Rh, Ir
Ir	Ru, Rh, Os, Pt
Pt	Cr, Ru, Rh, Pd, Ir

†The ordered $Li_4M_IM_{II}O_6$ compounds are marked with a purple-colored font.

Table S11. Suggested active-inactive cathode pairs†.

M in Li_2MO_3	Li_2MO_3 pairing (*utilized as*) active/inactive	inactive/active
Ti	*n/a*	Cr, Co, Ru, Rh, Pd, Os, Ir, Pt
V	Hf	*n/a*
Cr	Ti, Mn, Ge	Ru, Rh, Pd, Os, Ir, Pt
Mn	*n/a*	Cr, Co, Ru, Rh, Pd, Os, Ir, Pt
Fe	*n/a*	Ru, Rh, Os, Ir, Pt
Co	Ti, Mn, Ni, Ge	Ru, Rh, Pd, Ir
Ni	*n/a*	Co, Rh, Pd, Ir, Pt
Ge	*n/a*	Cr, Co, Ru, Rh, Pd, Ir, Pt
Zr	*n/a*	Pd, Ir
Ru	Ti, Cr, Mn, Fe, Co, Ge, Rh, Pd, Sn, Hf, Pt, Pb	*n/a*
Rh	Ti, Cr, Mn, Fe, Co, Ni, Ge, Pd, Sn, Hf	Ru, Os, Ir
Pd	Ti, Cr, Mn, Co, Ni, Ge, Zr, Sn, Hf	Ru, Rh, Os, Ir
Sn	*n/a*	Ru, Rh, Pd, Ir
Hf	*n/a*	V, Ru, Rh, Pd, Ir, Pt
Os	Ti, Cr, Mn, Fe, Rh, Pd, Pb	*n/a*
Ir	Ti, Cr, Mn, Fe, Co, Ni, Ge, Zr, Rh, Pd, Sn, Hf, Pt, Pb	*n/a*
Pt	Ti, Cr, Mn, Fe, Ni, Ge, Hf	Ru, Ir
Pb	*n/a*	Ru, Os, Ir

†The ordered $Li_4M_IM_{II}O_6$ compounds are marked with a purple-colored font. After screening, we find that there is no inactive Li_2MO_3 stabilizer that can match with Li_2MoO_3 active cathode (*i.e.*, they decompose to other stable phase mixtures).

S1. Methodology

We use density functional theory (DFT) as implemented in the Vienna Ab-initio Simulation Package (VASP)[37,38] for all the first-principles calculations reported in this work. We use projector-augmented wave (PAW)[39] potentials to model the ion-electron interactions, and the PBE parameterization of a generalized gradient approximation[41] to the exchange-correlation energy functional. We use a constant plane-wave cutoff energy of 520 eV, and a dense Γ-centered k-mesh corresponding to ~8,000 k-points per reciprocal atom (KPPRA) in the Brillouin zone to calculate total energies. We relax all structures fully with respect to cell volume and atomic positions until forces on all atoms are within a few meV/Å and stresses are within a few kbar. Any species with an unfilled *d*-orbital (*f*-orbital) is given an initial magnetic moment of $5\mu_B$ ($7\mu_B$) in a ferromagnetic configuration, and allowed to electronically relax to self-consistency. For compounds containing certain *d*- and *f*-block elements, we perform GGA+*U* calculations using the Dudarev approach,[42] and the corresponding *U*-*J* values are listed in Table S12.

We test the convergence of properties such as $\Delta E_O^{vac}, \Delta E_{TM}^{mig}$, and ΔE^{mix} with supercell size, by calculating them using supercells up to 32 formula units (*f.u.*). Our calculations indicate that for Li_2MnO_3, ΔE_O^{vac} calculated using $2 \times 1 \times 1$ supercell (with four *f.u.*) is within 5 meV/vacancy when compared to that calculated with a $Li_{64}Mn_{32}O_{96}$ supercell (with defects separated by ~10.2 Å). Similar tests on 'MMS'-MoO_3 as a function of supercell sizes find that ΔE_{TM}^{mig} is converged within 10 meV/Mo site. Lastly, we tested several metal orderings in a $2 \times 1 \times 1$ $Li_2Ru_{0.5}M_{0.5}O_3$ supercell (M = Ni, Ir, Ti, or Mn). We find that all of the lowest energy mixing configurations to have the ΔE^{mix} values that are consistent with the settings used for our high-throughput calculations.

S2. Additional notes on Li_2CoO_3 and Li_2CrO_3

● We have found the following papers mentioning "Li_2CoO_3"; however, they are typos in place of either $LiCoO_2$ (*i.e.*, one of the most common cathode materials) or Li_2CO_3 (*i.e.*, one of the most commonly used Li-containing precursors).

1) $LiCoO_2$

- Prachařová *et al.*, *J. Power Sources*, 2002, **108**, 204.
- Kozen *et al.*, *Chem. Mater.*, 2015, **27**, 5324.
- Guo *et al.*, *Waste Management*, 2016, **51**, 227.
- Ponce *et al.*, *J. Phys. Chem. C*, 2017, **121**, 12959.
- Liang *et al.*, *J. Power Sources*, 2017, **342**, 836.

2) Li_2CO_3

- Kim *et al.*, *Mater. Res. Bull.*, 1999, **34**, 571.
- Gendron *et al.*, *Solid State Ionics*, 2003, **157**, 125.
- Majumder *et al.*, *J. Power Sources*, 2006, **154**, 262.
- Fleutot *et al.*, *J. Power Sources*, 2008, **180**, 836.
- Luo *et al.*, *Nat. Chem.*, 2010, **2**, 760.
- Einarsrud *et al.*, *Chem. Soc. Rev.*, 2014, **43**, 2187.
- Khatun *et al.*, *J. Scientific Research*, 2014, **6**, 217.
- Sarker *et al.*, *Mater. Res.*, 2016, **19**, 505.
- Lu *et al.*, *RSC Adv.*, 2017, **7**, 4269.

● Additionally, we note that the Materials Project[35] contains two hypothetical Li_2CoO_3 structures (*i.e.*, *Pnnm* and *P4₂/mnm*) that are thermodynamically unstable with a convex hull distance of >90 meV/atom. We have also tested the hypothetical *C2/m* $Li_7Co_5O_{12}$ phase from the Materials Project.[35] We find that $Li_7Co_5O_{12}$ lies just above the convex hull (by ~2 meV/atom) with respect to other stable compounds present in Li-Co-O chemical space within the OQMD,[33,34] and thus does not affect the calculated stability of the *C2/m* Li_2CoO_3.

● To the best of our knowledge, there is only one mention of Li_2CrO_3 in the literature but there is no description of the compound at all; see Patil Shrinivas *et al.*, *International Journal of Current Trends in Engineering & Research*, 2016, **2**, 108.

● The Materials Project[35] contains eight hypothetical structures for Li_2CrO_3. The two lowest energy Li_2CrO_3 structures belong to the space group of *C2/c* and *C2/m* (with the hull distance of 6 and 19 meV/atom, respectively), consistent with our results, and suggesting that a Li-rich Li_2CrO_3 compound is likely to be stable yet to be experimentally synthesized.

S3. Properties of the top-30 active/inactive pair candidates in Table 1

● We define the gravimetric *"Energy density*" in Table 1 as the product of "*Average voltage*" of the composite redox window and "*Composite capacity*" of the $Li_2M_IO_3$-$Li_2M_{II}O_3$.

● The lower bound of composite "*Redox window*" in Table 1 corresponds to the lowest delithiation voltage of active $Li_2M_IO_3$ component (Fig. 2); and the upper bound corresponds to an activation voltage of inactive $Li_2M_{II}O_3$ (*i.e.*, lowest delithiation voltage of inactive $Li_2M_{II}O_3$ component).

● The "*Composite capacity*" in Table 1 is calculated by utilizing an accessible capacity from active $Li_2M_IO_3$ in $Li_2M_IO_3$-$Li_2M_{II}O_3$ composite (*i.e.*, within the "*Redox window*" shown in Table 1); in other words, we do not consider delithiating inactive $Li_2M_{II}O_3$ counterparts to calculate the final gravimetric energy density. In reality, the "*Composite capacity*" (and "*Energy density*") can increase upon activating its inactive $Li_2M_{II}O_3$ component, and also by tuning the active/inactive $Li_2M_{I(II)}O_3$ mole ratios in the composite (here, we consider 1:1 active/inactive mole ratio in Table 1).

● The relative "*Stability within OQMD*" (*i.e.*, convex-hull distance) in the Li-M_I-M_{II}-O phase diagram within the OQMD framework[33,34] is provided. All of the top-30 active/inactive pair cathode candidates are either on the convex-hull (*i.e.*, stable) or near the convex-hull (*i.e.*, nearly stable, ~25 meV/atom). It is expected that these predicted thermodynamically stable/nearly-stable compounds can be synthesized experimentally, as the currently known Li_4RuMO_6 (M = Ti, Mn, Sn) systems[14-18] have the convex-hull distance of 5, 17, and 17 meV/atom, respectively, in Table 1. For further discussions on "stability", please refer to Table S1, methods section, and/or *Refs.* 33 – 34.

Table S12. *U* values adapted from *Refs.* 33, 34

Li_2MO_3 (M = chemical element)	*U* value for M [eV]
Ti	*n/a*
V	3.1
Cr	3.5
Mn	3.8
Fe	4.0
Co	3.3
Ni	6.4
Ge	*n/a*
Zr	*n/a*
Mo	*n/a*
Ru	*n/a*
Rh	*n/a*
Pd	*n/a*
Sn	*n/a*
Hf	*n/a*
Os	*n/a*
Ir	*n/a*
Pt	*n/a*
Pb	*n/a*